Impact of Dispersion Effects on Temporal-Convolution-Based Real-Time Fourier Transformation Systems

Bowen Zhang, Dan Zhu, *Member, IEEE*, Zhen Lei, Zhongyang Xu, *Member, IEEE*, Tao Zhou, Xin Zhong, Zhiyu Chen, and Shilong Pan, *Senior Member, IEEE, Fellow, OSA*

***Abstract*—The impact of dispersion effects on temporal-convolution-based real-time Fourier transformation (RTFT) systems, including the residual 2nd-order dispersion effect, the 3rd-order dispersion effect, and their joint effect, is theoretically analyzed. To reduce these effects, an optical RTFT system based on a bidirectional chirped fiber Bragg grating (CFBG) and an optical filter is proposed. Only one optical pulse source, a bidirectional CFBG, a Mach–Zehnder modulator (MZM) and a photodetector (PD) are needed. RTFT with a bandwidth of 40 GHz and a frequency resolution of 0.7 GHz has been experimentally achieved.**

***Index Terms*—Dispersion, fiber Bragg grating, Fourier transformation, microwave photonics.**

I. Introduction

FOURIER transformation realizes the spectrum analysis of a temporal signal, which is of great importance in the RF systems of electronic warfare [1], radar [2], and wireless communication [3]. Benefiting from the advantages of low loss, large bandwidth and high processing speed introduced by photonic techniques, photonics-based real-time Fourier transformation (RTFT) has been extensively investigated. To date, numerous methods have been proposed to implement the photonics-based RTFT, which can be divided into three categories.

In the first category, the photonics-based RTFT is implemented using a dispersive medium [4]–[8], directly mapping the frequency spectrum to the time domain with the space-time duality. Similar to the Fourier transformation based on Fraunhofer diffraction in the space domain, RTFT in the time domain can be implemented based on the dispersion effect. This concept was first proposed in [4], and the dispersive medium can be realized by a length of single-mode fiber (SMF) [5] or dispersion compensation fiber [6]. To improve the frequency resolution of the RTFT system, a fiber grating with a large 2nd-order dispersion value is used to act as the dispersive medium [7]–[11]. It is worthy to note that the temporal far-field condition must be satisfied, i.e., an optical pulse with a very narrow time duration and a dispersive medium with a large dispersion value are required. When the dispersion value is not large enough, to satisfy the temporal far-field condition, time lens can be applied, which provides a quadratic phase to match the chirp induced by the dispersion [12]–[17]. The dispersion-based RTFT method is simple in structure and has the advantage of large instantaneous bandwidth up to several terahertz. However, the frequency-to-time mapping coefficient of the system is limited by the dispersion value. Thus the frequency resolution of the system is usually poor. This method is usually used in the measurement of the optical spectrum.

In order to improve the frequency resolution, in the second category, a frequency-shifted loop (FSL) [18]–[23] is employed to implement the photonics-based RTFT. The FSL is usually composed of an optical filter, an optical frequency shifter, an optical time delay line, and a gain medium. When an optical signal is injected into the loop, time shift and frequency shift are simultaneously added to the signal in each cycle. By properly setting the time delay and the shifted frequency in the FSL, all the replicas are summed together at the output of the loop. The mathematical expression of the output signal is exactly the Fourier transformation definition of the injected optical signal. This method realizes an extremely high resolution of several kilohertz, which overcomes the frequency-resolution limitations of the dispersion-based RTFT schemes. However, the non-overlapping bandwidth of this method is limited to only tens of megahertz, as large as that of the frequency shift in the loop, which is not applicable for the broadband microwave signal measurement.

In order to realize a large bandwidth and a fine resolution at the same time, a temporal convolution system [24]–[26] based on temporal pulse shaping [27]–[30] is introduced. In this method, an ultra-short optical pulse passes through a temporal stretching medium, a Mach-Zehnder modulator (MZM) and a temporal

Manuscript received March 10, 2020; revised May 2, 2020; accepted May 5, 2020. Date of publication May 11, 2020; date of current version September 1, 2020. This work was supported in part by National Key R&D Program of China (2018YFB2201803), in part by National Natural Science Foundation of China under Grant 61971222, in part by the Jiangsu Provincial Program for High-level Talents in Six Areas under Grant DZXX-030, and in part by the Fundamental Research Funds for Central Universities under Grant NE2017002 and Grant NC2018005. *(Corresponding authors: Dan Zhu; Shilong Pan.)*

The authors are with the Key Laboratory of Radar Imaging and Microwave Photonics, Ministry of Education, Nanjing University of Aeronautics and Astronautics, Nanjing 210016, China (e-mail: bwzhang@nuaa.edu.cn; danzhu@nuaa.edu.cn; leizhen@nuaa.edu.cn; xzy@nuaa.edu.cn; zhj_zht@163.com; 15497546@qq.com; chenzhiyu_1986@163.com; pans@ieee.org).

Color versions of one or more of the figures in this article are available online at https://ieeexplore.ieee.org.

Digital Object Identifier 10.1109/JLT.2020.2993608

compression medium. If the operations of temporal stretching and temporal compression are complementary, the spectrum of the electrical signal applied to the modulator is mapped into the time domain at the output of the system. Thus, the schemes in this category can be used in ultrafast electrical spectrum analyzers [31] and compressive receivers for multiple-frequency measurement [32]. However, an oscilloscope with a high sampling rate is required to observe the output result. In order to reduce this requirement, the technologies of temporal amplification [33] and asynchronous optical sampling [34] are proposed. However, the current schemes have the following issues which have not been analyzed in depth: first, the optimal frequency resolution needs the match of the dispersion values before and after the modulator, which is hard to achieve in the previous works; second, the effect of amplitude fading versus microwave frequency exists in the previous experimental results, which is unignorable for signal measurement over large bandwidth; finally, the amplitudes of the sideband pulses, which appear at the two sides of the middle reference pulse in the RTFT result, are not equal, bringing distortion to the accuracy of the measurement.

In this work, we theoretically analyze the causes of the above phenomena. The mismatch of the 2nd-order dispersions for temporal stretching and compression causes the broadening of the signal pulses in RTFT results, which will bring a degraded frequency resolution. The frequency-dependent modulation depth at the MZM and the existence of the 3rd-order dispersion cause the amplitude fading effect. The joint effect of the 2nd-order dispersion mismatch and the existence of the 3rd-order dispersion causes the amplitude imbalance of the output sideband pulses. In order to solve these problems, a bidirectional CFBG, which offers complementary dispersions for the optical pulses propagating in the two opposite directions, is utilized to realize the match of the 2nd-order dispersion. Precise dispersion management to eliminate the 3rd-order dispersion in the system, as well as a post-processing method utilizing the modulator responses at different frequencies, can be used to compensate for the amplitude fading. The amplitude imbalance of the sideband pulses appearing at the two sides of the reference pulse can be reduced by using an optical filter after the laser source.

Based on these methods, a photonics-based RTFT system is designed. In the system, an optical pulse is filtered by an optical filter, temporally stretched and compressed in the same CFBG. Using an electro-optical modulator, the electrical signal to be measured is modulated to the stretched optical pulse and the spectrum of the electrical signal will be mapped into the time domain. By analyzing the output temporal waveform with post-processing, the frequency information of the electrical signal can be obtained with an optimal resolution. Mathematical analysis of the impact of the dispersion effects on the temporal-convolution-based RTFT system is given based on the constructed model. Simulations and corresponding experimental demonstrations are also carried out. In the experiment, a frequency resolution of 0.7 GHz and a bandwidth of 40 GHz have been experimentally verified. Meanwhile, this system has the ability to realize the ultrafast frequency measurement with an acquisition frame rate of 10 MHz.

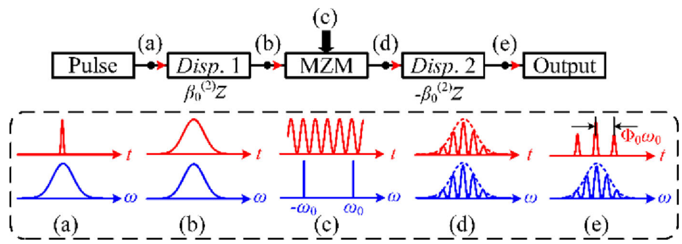

Fig. 1. Schematic diagram of the traditional photonics-based RTFT system. *Disp*. 1: the first dispersion medium, MZM: Mach-Zehnder modulator, *Disp*. 2: the second dispersion medium. Red curves: temporal waveforms of the optical signals or the electrical signals; blue curves: corresponding spectra.

II. Principle and Theoretical Analysis

A. Principle of Traditional Photonics-Based RTFT

The schematic diagram of a traditional photonics-based RTFT system is shown in Fig. 1. An ultra-narrow optical pulse with an ultra-wideband spectrum is injected into the first dispersion medium (*Disp*. 1) and is stretched in the time domain. Then the temporally stretched optical pulse is modulated by the electrical signal to be Fourier transformed at an MZM. The optical output of the MZM is injected into the second dispersion medium (*Disp*. 2). The 2nd-order dispersion values of *Disp*. 1 and *Disp*. 2 are equal but with opposite signs, which are $\beta_0{}^{(2)}z$ and $-\beta_0{}^{(2)}z$, respectively. Thus the pulse is recompressed and the spectrum of the electrical signal is mapped into the time domain. In this way, the RTFT process is accomplished.

Mathematically, the ultra-narrow optical pulse can be expressed as $u_0(t)$ with a time width of δ_τ and a repetition period of T_0. The spectrum of $u_0(t)$ is written as $U_0(\omega)$. The transfer functions and impulse response functions of *Disp*. 1 and *Disp*. 2 can be described as $H_1(\omega)$, $H_2(\omega)$, $h_1(t)$, $h_2(t)$, respectively, with the expressions given by

$$\begin{cases} H_1(\omega) = \exp\left(-j\dfrac{\beta_0{}^{(2)}z}{2}\omega^2\right) \\ H_2(\omega) = \exp\left(+j\dfrac{\beta_0{}^{(2)}z}{2}\omega^2\right) \\ h_1(t) = \dfrac{1}{\sqrt{+j2\pi\beta_0{}^{(2)}z}}\exp\left(+j\dfrac{1}{2\beta_0{}^{(2)}z}t^2\right) \\ h_2(t) = \dfrac{1}{\sqrt{-j2\pi\beta_0{}^{(2)}z}}\exp\left(-j\dfrac{1}{2\beta_0{}^{(2)}z}t^2\right) \end{cases} \tag{1}$$

With the ultra-narrow optical pulse $u_0(t)$ injected into *Disp*. 1, the optical pulse is temporally stretched and spectrally dispersed, which can be written as

$$\begin{aligned} u_1(t) &= u_0(t)\otimes h_1(t) \\ &= \frac{1}{\sqrt{+j2\pi\beta_0{}^{(2)}z}}\int_{-\infty}^{+\infty} u_0(\tau)\exp\left(j\frac{1}{2\beta_0{}^{(2)}z}(t-\tau)^2\right)d\tau \\ &= \frac{1}{\sqrt{+j2\pi\beta_0{}^{(2)}z}}\exp\left(j\frac{1}{2\beta_0{}^{(2)}z}t^2\right)U_0\left(\frac{t}{\beta_0{}^{(2)}z}\right) \end{aligned} \tag{2}$$

The temporally stretched optical pulse is then injected into an MZM and modulated by the electrical signal to be Fourier transformed. The electrical signal is expressed as $V_m s(t)$, where V_m is the amplitude and $s(t)$ is the normalized modulated signal. Assuming that $V_m s(t)$ is a small signal, the output of the MZM is given by

$$\begin{cases} u_2(t) \approx u_1(t) \times s'(t) \\ s'(t) = [a + b\beta_m s(t)] \end{cases} \tag{3}$$

where $\beta_m = \pi V_m / V_\pi$ is the modulation depth and V_π is the half-wave voltage of the MZM, a and b correspond to the relative amplitudes of the optical carrier and the $\pm 1^{\text{st}}$-order sidebands, respectively, which can be adjusted by changing the bias voltage of the modulator. The output of the MZM is injected into *Disp*. 2 and experiences the dispersion with the value of $-\beta_0{}^{(2)}z$. The output from port 2 of the bidirectional CFBG in the time domain is then expressed as

$$\begin{aligned} u_3(t) &= u_2(t) \otimes h_2(t) \\ &= a u_0(t) + b\beta_m \exp\left(-j\frac{1}{2\beta_0{}^{(2)}z}t^2\right) u_0(t) \\ &\quad \otimes S\left(-\frac{t}{\beta_0{}^{(2)}z}\right) \end{aligned} \tag{4}$$

where $S(\omega)$ is the spectrum of $s(t)$. As can be seen, when the temporal stretching and the compression are ideally complementary, the output field is the combination of the original pulse, serving as the reference pulse, and the convolution between the original optical pulse and the scaled spectrum of $S(\omega)$, serving as the signal pulse.

Especially, when the modulated signal is a single-frequency signal with a frequency of f, $S'(\omega)$, which is the spectrum of $s'(t)$ in (3), can be written as $S'(\omega) = a\delta(\omega) + b\beta_m\delta(\omega + 2\pi f)/2 + b\beta_m\delta(\omega - 2\pi f)/2$. Thus the spectrum of $u_3(t)$ is obtained,

$$\begin{aligned} U_3(\omega) &= \{[U_0(\omega) \times H_1(\omega)] \otimes S'(\omega)\} \times H_2(\omega) \\ &= aU_0(\omega) \\ &\quad + b\frac{\beta_m}{2}U_0(\omega - 2\pi f) \\ &\quad \exp\left\{j\frac{\beta_0{}^{(2)}z}{2}\left[(2\pi f)^2 - 2(2\pi f)\omega\right]\right\} \\ &\quad + b\frac{\beta_m}{2}U_0(\omega + 2\pi f) \\ &\quad \exp\left\{j\frac{\beta_0{}^{(2)}z}{2}\left[(2\pi f)^2 + 2(2\pi f)\omega\right]\right\} \end{aligned} \tag{5}$$

The temporal waveform of $u_3(t)$ can be calculated from (5),

$$\begin{aligned} u_3(t) &= IF[U_3(\omega)] \\ &= a u_0(t) \\ &\quad + b\frac{\beta_m}{2}\exp\left(-j\frac{\beta_0{}^{(2)}z}{2}(2\pi f)^2\right) \\ &\quad \exp(-j2\pi f t)\, u_0\left(t + 2\pi\beta_0{}^{(2)}zf\right) \\ &\quad + b\frac{\beta_m}{2}\exp\left(-j\frac{\beta_0{}^{(2)}z}{2}(2\pi f)^2\right) \\ &\quad \exp(+j2\pi f t)\, u_0\left(t - 2\pi\beta_0{}^{(2)}zf\right) \end{aligned} \tag{6}$$

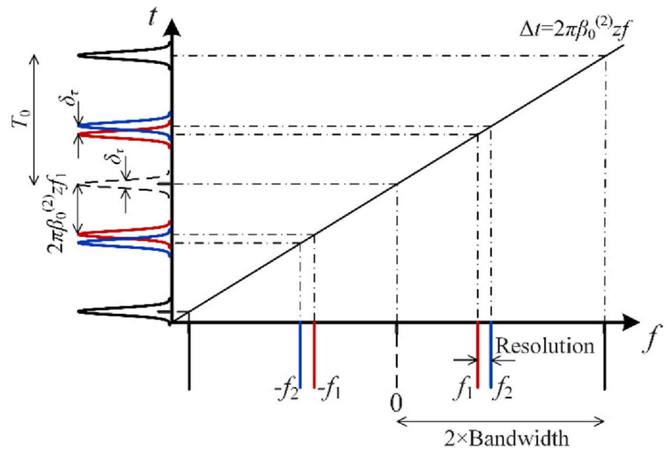

Fig. 2. Diagram of the relationship between the output waveform of the photonics-based RTFT system and the frequency of the modulated microwave signal.

where $IF(*)$ is the process of inverse Fourier transformation. As can be seen, when the modulated signal is a single-frequency signal, there are three copies of the original pulse at the output. According to (6), Fig. 2 is plotted to reveal the relationship between the output waveform of the photonics-based RTFT system and the frequency of the modulated microwave signal. As can be seen, the output waveform contains one reference pulse and two signal pulses. The signal pulse is exactly the time-shifted reference pulse, which is plotted as the dashed line. The time delay between the reference pulse and the signal pulse can be expressed as $\Delta t = 2\pi\beta_0{}^{(2)}zf$. On one hand, the frequency resolution of the RTFT system refers to the minimum frequency difference that can be discriminated, which is determined by the temporal width of the output reference pulse. On the other hand, the operational bandwidth of the RTFT system refers to the non-overlapping frequency measurement range of the microwave signal. When double-sideband modulation is applied, the bandwidth of the system is the ratio between half of the output reference pulse period and the frequency-to-time mapping factor. As a result, the theoretical frequency resolution of this system is $\delta_\tau / 2\pi\beta_0^{(2)}z$, and the bandwidth is $T_0/4\pi\beta_0{}^{(2)}z$.

B. Effect of the Residual 2nd-Order Dispersion

The effect of the residual 2^{nd}-order dispersion is analyzed. Assuming that the dispersions before and after the modulator are slightly different, i.e., the dispersion value after the modulator is $-\beta_0{}^{(2)}z + \Delta\beta^{(2)}z$ and $\Delta\beta^{(2)}z << \beta_0{}^{(2)}z$. The model of the system can be described as Fig. 3. A residual dispersion medium *Disp.* 3 with the 2^{nd}-order dispersion value of $\Delta\beta^{(2)}z$, is introduced after *Disp.* 2. Similarly, the transfer function and impulse response function of *Disp*. 3 can be expressed as $H_3(\omega) =$

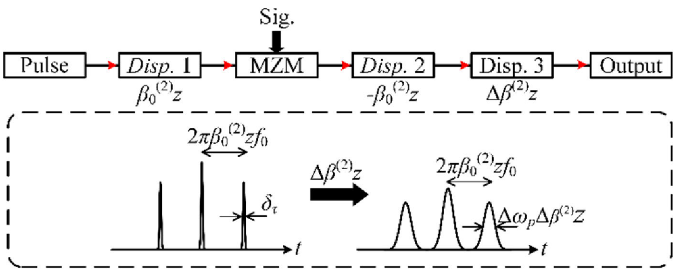

Fig. 3. Schematic diagram of the RTFT system consisting of the residual 2nd-order dispersion, *Disp*. 3.

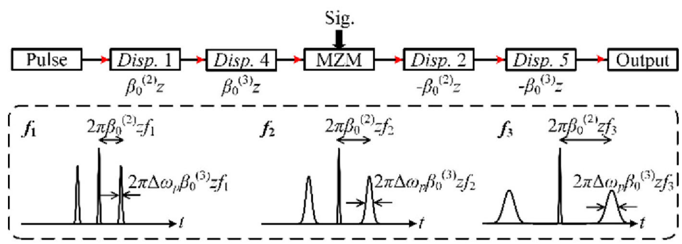

Fig. 4. Schematic diagram of the RTFT system consisting of the 3rd-order dispersions, *Disp*. 4 and *Disp*. 5.

$\exp(-j\Delta\beta^{(2)}z\omega^2/2)$ and $h_3(t) = \exp(jt^2/2\Delta\beta^{(2)}z)/(j2\pi\Delta\beta^{(2)}z)^{1/2}$, respectively. Mathematically, the signal output from *Disp*. 3 can be expressed as

$$\begin{aligned}
u_4(t) &= IF\left\{\left[\left(U_0(\omega)H_1(\omega)\right)\otimes S'(\omega)\right]H_2(\omega)H_3(\omega)\right\}\\
&= a\frac{1}{\sqrt{+j2\pi\Delta\beta^{(2)}z}}\exp\left(j\frac{1}{2\Delta\beta^{(2)}z}t^2\right)U_0\left(\frac{t}{\Delta\beta^{(2)}z}\right)\\
&\quad + b\frac{\beta_m}{2}\frac{1}{\sqrt{+j2\pi\Delta\beta^{(2)}z}}\exp\left(j\frac{\beta_0{}^{(2)}z}{2}(2\pi f)^2\right)\\
&\quad \exp\left(j\frac{\left(t+2\pi\beta_0{}^{(2)}zf\right)^2}{2\Delta\beta^{(2)}z}\right)U_0\left(\frac{t+2\pi\beta_0{}^{(2)}zf}{\Delta\beta^{(2)}z}-2\pi f\right)\\
&\quad + b\frac{\beta_m}{2}\frac{1}{\sqrt{+j2\pi\Delta\beta^{(2)}z}}\exp\left(j\frac{\beta_0{}^{(2)}z}{2}(2\pi f)^2\right)\\
&\quad \exp\left(j\frac{\left(t-2\pi\beta_0{}^{(2)}zf\right)^2}{2\Delta\beta^{(2)}z}\right)U_0\left(\frac{t-2\pi\beta_0{}^{(2)}zf}{\Delta\beta^{(2)}z}+2\pi f\right)
\end{aligned}\tag{7}$$

As can be seen, there is a slight shift with the time delay between the reference pulse and the signal pulse. The value of this shift is $2\pi\Delta\beta^{(2)}zf$, which can be ignored when $\Delta\beta^{(2)}z << \beta_0{}^{(2)}z$. An amplitude fading with a factor of $1/(2\pi\Delta\beta^{(2)}z)^{1/2}$ is also introduced to the output pulses. At the same time, the reference pulse and the signal pulses are temporal mappings from the spectrum of the original optical pulse with the same mapping factor of $\Delta\beta^{(2)}z$. Thus all the reference and signal pulses are broadened and the temporal widths of the pulses are approximately $\Delta\omega_p\Delta\beta^{(2)}z$, where $\Delta\omega_p$ is the spectrum bandwidth of the original optical pulse. As a result, the frequency resolution of the photonics-based RTFT system will be degraded to be $\Delta\omega_p\Delta\beta^{(2)}z/2\pi\beta_0^{(2)}z$. As can be seen, the frequency resolution of the RTFT system depends on the match degree of the 2nd-order dispersions before and after the modulator. In order to achieve an optimal frequency resolution, an ideal match of the dispersions is highly required.

C. Effect of the 3rd-Order Dispersion

Another important factor that may influence the performance of the photonics-based RTFT system is the 3rd-order dispersion. As shown in Fig. 4, it is assumed that there exist 3rd-order dispersions expressed as *Disp.* 4 and *Disp.* 5 with the values of $\beta_0{}^{(3)}z$ and $-\beta_0{}^{(3)}z$-$\Delta\beta^{(3)}z$, respectively. The corresponding transfer functions of *Disp.* 4 and *Disp.* 5 can be expressed as $H_4(\omega) = exp(-j\beta_0{}^{(3)}z\omega^3/6)$ and $H_5(\omega) = exp(j\beta_0{}^{(3)}z\omega^3/6 + j\Delta\beta^{(3)}z\omega^3/6)$. Thus the output signal can be written as

$$\begin{aligned}
u_5(t) &= IF\left\{\left[\left(U_0(\omega)H_1(\omega)U_4(\omega)\right)\otimes S(\omega)\right]H_2(\omega)H_5(\omega)\right\}\\
&= IF\left[\exp\left(j\Delta\beta^{(3)}z\omega^3\big/6\right)\right]\otimes\\
&\left\{\begin{array}{l}
au_0(t)\\
+b\frac{\beta_m}{2}\frac{1}{\sqrt{-j2\pi\beta_0{}^{(3)}z(2\pi f)}}\\
\times\exp\left(-j\frac{\beta_0{}^{(2)}z}{2}(2\pi f)^2 - j\frac{\beta_0{}^{(3)}z}{6}(2\pi f)^3\right)\\
\times\exp\left(j\frac{\left(t+\beta_0{}^{(2)}z(2\pi f)+\beta_0{}^{(3)}z(2\pi f)^2/2\right)^2}{2\beta_0{}^{(3)}z(2\pi f)}\right)\\
\times U_0\left(\frac{t+\beta_0{}^{(2)}z(2\pi f)+\beta_0{}^{(3)}z(2\pi f)^2/2}{-\beta_0{}^{(3)}z(2\pi f)} - 2\pi f\right)\\
+b\frac{\beta_m}{2}\frac{1}{\sqrt{+j2\pi\beta_0{}^{(3)}z(2\pi f)}}\\
\times\exp\left(-j\frac{\beta_0{}^{(2)}z}{2}(2\pi f)^2 + j\frac{\beta_0{}^{(3)}z}{6}(2\pi f)^3\right)\\
\times\exp\left(j\frac{\left(t-\beta_0{}^{(2)}z(2\pi f)+\beta_0{}^{(3)}z(2\pi f)^2/2\right)^2}{-2\beta_0{}^{(3)}z(2\pi f)}\right)\\
\times U_0\left(\frac{t-\beta_0{}^{(2)}z(2\pi f)+\beta_0{}^{(3)}z(2\pi f)^2/2}{\beta_0{}^{(3)}z(2\pi f)} + 2\pi f\right)
\end{array}\right\}
\end{aligned}\tag{8}$$

The first term of (8) is due to the mismatch of the 3rd-order dispersions in the system, which will bring distortions to the shape, amplitude, and pulse width of the output pulses [35]. The distortions of the output pulses are related to the type of the original pulse and the value of the residual 3rd-order dispersion, i.e., $\Delta\beta^{(3)}z$. When $\Delta\beta^{(3)}z$ is very small, the distortions brought by the mismatch of the 3rd-order dispersions can be ignored. Under this condition, the first term of (8) will disappear, and the second term indicates a slight time delay shift between the reference and signal pulses when the 3rd-order dispersions exist. The value of this shift is $3\beta_0{}^{(3)}z(2\pi f)^2/2$, which can be ignored when $\beta_0{}^{(3)}z(2\pi f) << \beta_0{}^{(2)}z$. At the same time, the signal pulses are broadened and the temporal widths of the pulses are approximately $\Delta\omega_p\beta_0^{(3)}z(2\pi f)$, as shown in Fig. 4. Consequently, the frequency resolution of the photonics-based RTFT system will be degraded to be $\Delta\omega_p\beta_0^{(3)}z(2\pi f)/2\pi\beta_0^{(2)}z$. Compared with the effect of the residual 2nd-order dispersion,

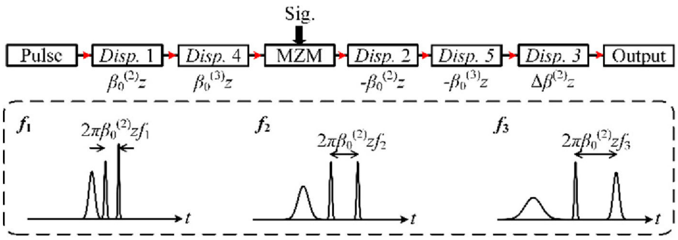

Fig. 5. Schematic diagram of the RTFT system consisting of the residual 2nd-order dispersion, *Disp*. 3, and the 3rd-order dispersions, *Disp*. 4 and *Disp*. 5.

the broadening of the signal pulses caused by the 3rd-order dispersion is frequency-dependent. With the increase of the modulated microwave signal frequency, the broadening of the signal pulses will increase, resulting in a degraded frequency resolution. In addition, a frequency-dependent amplitude fading with a factor of $1/(2\pi\beta_0{}^{(3)}z(2\pi f))^{1/2}$ will also be introduced to the signal pulses.

D. Joint Effect of the Residual 2nd-Order Dispersion and the 3rd-Order Dispersion

In Part *B* and Part *C*, the separate influences of the residual 2nd-order dispersion and the 3rd-order dispersion on the performance of the photonics-based RTFT system are analyzed. In this part, both the residual 2nd-order dispersion and the 3rd-order dispersion are taken into consideration. A more general model of the photonics-based RTFT system is established, as shown in Fig. 5. *Disp.* 4 and *Disp.* 5, acting as the dispersive medium with the 3rd-order dispersion value of $\beta_0{}^{(3)}z$ and $-\beta_0{}^{(3)}z-\Delta\beta^{(3)}z$, are added, as well as the residual 2nd-order dispersion medium *Disp.* 3 with the value of $\Delta\beta^{(2)}z$. The output signal is expressed as

$$
\begin{aligned}
u_5(t) &= IF\left\{\left[\left(U_0(\omega)H_1(\omega)U_4(\omega)\right)\otimes\right.\right.\\
&\qquad\left.\left. S(\omega)\right]H_2(\omega)H_5(\omega)H_3(\omega)\right\}\\
&= IF\left[\exp\left(j\Delta\beta^{(3)}z\omega^3\Big/6\right)\right]\otimes\\
&\left\{\begin{array}{l}
a\frac{1}{\sqrt{j2\pi\Delta\beta^{(2)}z}}\exp\left(j\frac{1}{2\Delta\beta^{(2)}z}t^2\right)U_0\left(\frac{t}{\Delta\beta^{(2)}z}\right)\\
+b\frac{\beta_m}{2}\frac{1}{\sqrt{-j2\pi\left(\beta_0{}^{(3)}z(2\pi f)+\Delta\beta^{(2)}z\right)}}\\
\times\exp\left(-j\frac{\beta_0{}^{(2)}z}{2}(2\pi f)^2-j\frac{\beta_0{}^{(3)}z}{6}(2\pi f)^3\right)\\
\times\exp\left(j\frac{\left(t+\beta_0{}^{(2)}z(2\pi f)+\beta_0{}^{(3)}z(2\pi f)^2/2\right)^2}{2\beta_0{}^{(3)}z(2\pi f)+2\Delta\beta^{(2)}z}\right)\\
\times U_0\left(\frac{t+\beta_0{}^{(2)}z(2\pi f)+\beta_0{}^{(3)}z(2\pi f)^2/2}{-\beta_0{}^{(3)}z(2\pi f)-\Delta\beta^{(2)}z}-2\pi f\right)\\
+b\frac{\beta_m}{2}\frac{1}{\sqrt{+j2\pi\left(\beta_0{}^{(3)}z(2\pi f)-\Delta\beta^{(2)}z\right)}}\\
\times\exp\left(-j\frac{\beta_0{}^{(2)}z}{2}(2\pi f)^2+j\frac{\beta_0{}^{(3)}z}{6}(2\pi f)^3\right)\\
\times\exp\left(j\frac{\left(t-\beta_0{}^{(2)}z(2\pi f)+\beta_0{}^{(3)}z(2\pi f)^2/2\right)^2}{-2\beta_0{}^{(3)}z(2\pi f)+2\Delta\beta^{(2)}z}\right)\\
\times U_0\left(\frac{t-\beta_0{}^{(2)}z(2\pi f)+\beta^{3}z(2\pi f)^2/2}{\beta_0{}^{(3)}z(2\pi f)-\Delta\beta^{(2)}z}+2\pi f\right)
\end{array}\right\}
\end{aligned}
\tag{9}
$$

Similar to (8), the first term of (9) also comes from the mismatch of the 3rd-order dispersions in the system, which can be ignored when $\Delta\beta^{(3)}z$ is small. Under this condition, as can be seen from the second term of (9), with the existence of the residual 2nd-order dispersion and the 3rd-order dispersion, a slight time delay shift appears between the reference pulse and the signal pulse. The value of this shift is $3\beta_0{}^{(3)}z(2\pi f)^2/2+2\pi\Delta\beta^{(2)}zf$, which can be ignored when $\beta_0{}^{(3)}z(2\pi f)<<\beta_0{}^{(2)}z$ and $\Delta\beta^{(2)}z<<\beta_0{}^{(2)}z$. At the same time, the reference pulse and signal pulses are broadened and the temporal widths are given by $\Delta\omega_p\Delta\beta^{(2)}z$, $\Delta\omega_p|\beta_0^{(3)}z(2\pi f)+\Delta\beta^{(2)}z|$ and $\Delta\omega_p|\beta_0^{(3)}z(2\pi f)-\Delta\beta^{(2)}z|$, respectively. At the same time, frequency-dependent amplitude fading is introduced to the signal pulses, as shown in Fig. 5. The frequency-dependent amplitude fading factors for the left and right signal pulses are $1/(2\pi|\beta_0{}^{(3)}z(2\pi f)+\Delta\beta^{(2)}z|)^{1/2}$ and $1/(2\pi|\beta_0{}^{(3)}z(2\pi f)-\Delta\beta^{(2)}z|)^{1/2}$, respectively. Thus the amplitude imbalance of the signal pulses located at the two sides of the reference pulse will exist.

According to the above analyses, the effect of dispersion in the temporal-convolution-based RTFT system can be summarized as follows: the value of the 2nd-order dispersion determines the frequency-to-time mapping coefficient of the system; the value of the residual 2nd-order dispersion causes the broadening of the output pulses, which will cause a degraded frequency resolution; the existence of the 3rd-order dispersion causes a frequency-dependent resolution degradation and the frequency-dependent amplitude fading of the output pulses; the joint effect of the residual 2nd-order dispersion and the 3rd-order dispersion introduces the frequency-dependent broadening of the signal pulses and the amplitude imbalance of the signal pulses located at the two sides of the reference pulse.

III. Simulation

In order to verify the principle, simulations are carried out based on the model shown in Fig. 5. The bandwidth of the optical pulse emitted from the pulse source is set to be 40 nm, and the dispersion values of *Disp.* 1 and *Disp.* 2 are set to be 2000 ps/nm and -2000 ps/nm, respectively, satisfying the characteristics of the CFBG in the subsequent experiment. The original optical pulse is assumed to be a transform-limited pulse with a Gaussian shape and a temporal width of 0.18 ps.

Firstly, *Disp.* 4 and *Disp.* 5 are set to be 0, i.e., only the residual 2nd-order dispersion is considered. When the dispersions for temporal stretching and compression are ideally complementary, i.e., the value of *Disp.*3 is 0, Fig. 6(a) shows the output waveform of the RTFT result of a 5-GHz microwave signal. The time width of the recompressed pulse is 0.18 ps, exactly the same as that of the original optical pulse. Thus the frequency resolution is calculated to be 11.25 MHz. As a comparison, when a residual 2nd-order dispersion exists with the value set to be 1 ps/nm, the corresponding output waveform is shown in Fig. 6(b). The time width of the recompressed pulse extends to be 40.18 ps, revealing a frequency resolution of 2.5 GHz. By changing the value of the residual 2nd-order dispersion *Disp.*3, the time width of the output signal pulse and the corresponding frequency resolution versus the residual 2nd-order dispersion value are simulated, with the

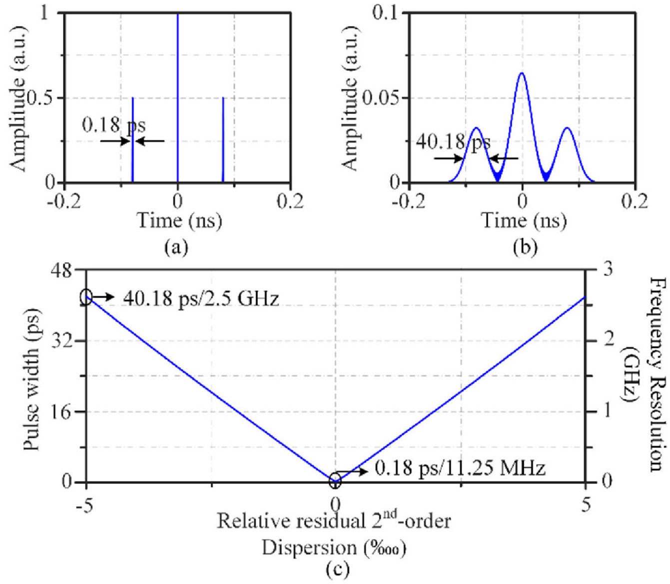

Fig. 6. The simulated RTFT results of a 5-GHz signal under the condition of (a) ideal dispersion compensation and (b) the existence of a residual 2nd-order dispersion with the value of 1 ps/nm. (c) Relationship between the time width of the output signal pulse, system resolution and the relative residual 2nd-order dispersion in the system.

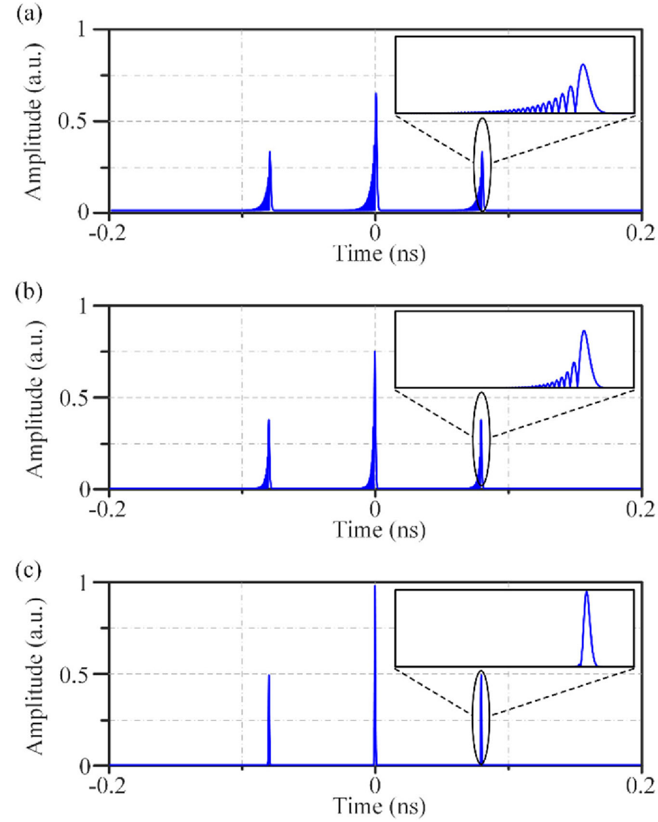

Fig. 7. The simulated RTFT results of a 5-GHz signal under the condition that the value of the residual 3rd-order dispersion is set to be (a) 5×10^{-3} ps/nm^2, (b) 1×10^{-3} ps/nm^2, (c) 1×10^{-4} ps/nm^2.

results shown in Fig. 6(c). It can be seen that the time width of the output signal pulse increases linearly with the residual 2nd-order dispersion value, and the frequency resolution of the system deteriorates, verifying the analyses provided in (7).

Then the effect of the residual 3rd-order dispersion is simulated. *Disp.* 3, *Disp.* 4 are all set to be 0. The value of *Disp.* 5 is changed from 5×10^{-3} ps/nm^2 to be 1×10^{-3}, 1×10^{-4} ps/nm^2. When a 5-GHz microwave signal is applied, the corresponding RTFT results are shown in Fig. 7. As can be seen, due to the effect of the residual 3rd-order dispersion, distortions are introduced to all the reference and signal pulses, verifying the theoretical analysis in (8). A larger value of the residual 3rd-order dispersion corresponds to a larger distortion. Fortunately, the residual 3rd-order dispersion in most RTFT systems is very small, which can usually be ignored. Besides, the distortions can also be decreased by reducing the spectrum bandwidth of the optical pulse. As a result, in the following simulations, the effect of the residual 3rd-order dispersion is not taken into consideration.

The effect of the 3rd-order dispersion with the RTFT results are also simulated. *Disp.* 3 is set to be 0 to guarantee an ideal match of the 2nd-order dispersions in the system. When there is no 3rd-order dispersion, Fig. 8(a) shows the RTFT results of the single-frequency signal with the frequency varying from 1 to 40 GHz. Then, *Disp.* 4 and *Disp.* 5 are set to be 0.1 ps/nm^2 and -0.1 ps/nm^2. The corresponding RTFT results of the single-frequency signal with the frequency varying from 1 to 40 GHz are shown in Fig. 8(b), where the red dashed curve represents the envelope. As can be seen, when the 3rd-order dispersion exists in the RTFT system, a frequency-dependent pulse broadening and amplitude fading is introduced. By changing the values of *Disp.* 4 and *Disp.* 5 from ±0.1 ps/nm^2 to be ±0.2, ±0.3, and ±0.4 ps/nm^2, envelopes are recorded and shown in Fig. 8(c). At the same time, the temporal widths of the output pulses are also calculated, with the results shown in Fig. 8(d). It can be seen that the broadening of the signal pulses increases with the frequency of the modulated microwave signal and the value of the 3rd-order dispersion, which causes a degraded frequency resolution and a lower amplitude of the output pulses. The simulation results verify the analyses provided in (8).

Finally, the joint effect of the residual 2nd-order dispersion and the 3rd-order dispersion is also verified. In the simulation, the value of *Disp.* 3 is set to be 0.02 ps/nm. When the values of *Disp.* 4 and *Disp.* 5 are ±0.1 ps/nm^2, with the frequency of the microwave signal varying from 1 GHz to 40 GHz, the envelope of the output waveform is plotted as the red curve in Fig. 9(a). As can be seen, besides the pulse broadening and the amplitude fading, the amplitude imbalance of output signal pulses located at the two sides of the reference pulse, is also introduced. The simulated results agree well with the analyses shown in Fig. 5 and (9). By changing the values of *Disp.* 4 and *Disp.* 5 from ±0.1 ps/nm^2 to be ±0.2, ±0.3, and ±0.4 ps/nm^2, the RTFT results of the single-frequency signal with the frequency varying from 1 to 40 GHz are obtained. The corresponding envelopes are also shown in Fig. 9(a). When the value of *Disp.* 3 is changed to be -0.01 ps/nm, the corresponding envelopes in Fig. 9(a) are changed, of which the curves are shown in Fig. 9(b). Fig. 9 shows

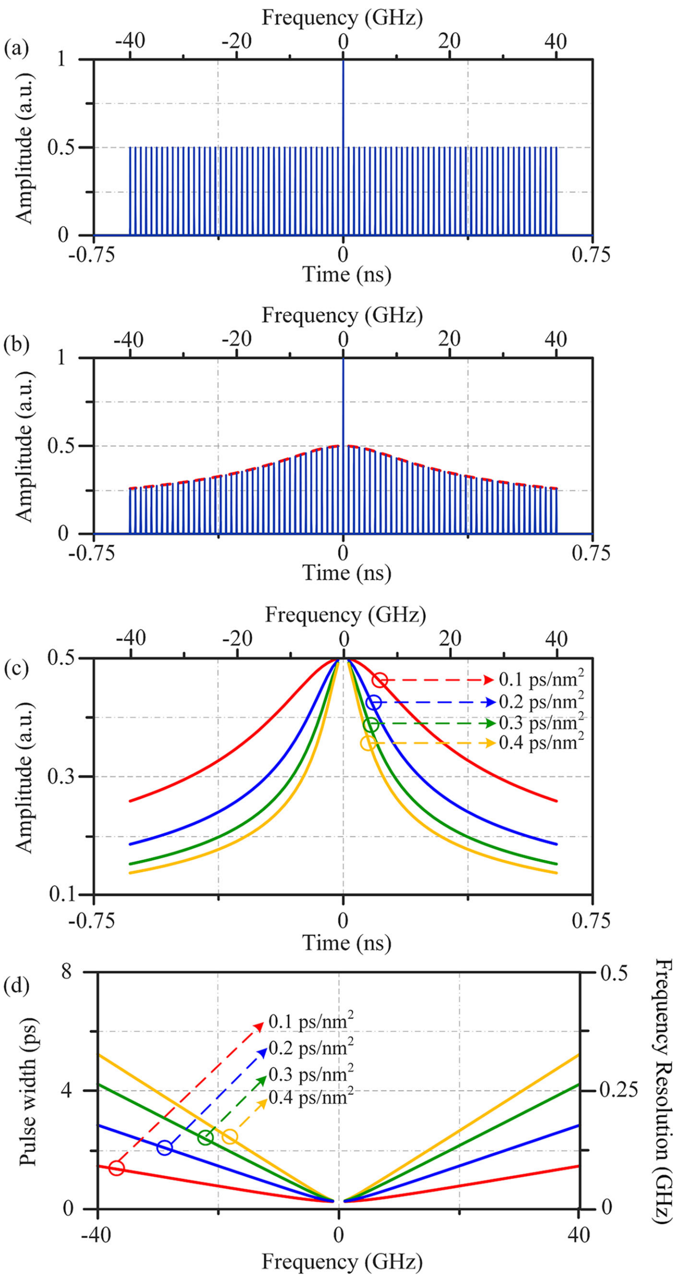

Fig. 8. The simulated RTFT results of a single-frequency signal with the frequency varying from 1 to 40 GHz when the values of the 3rd-order dispersions are set to be (a) 0 ps/nm^2 and (b) $\pm$0.1 ps/nm^2. The corresponding (c) envelopes, (d) pulse widths and frequency resolutions of the RTFT results when the values of the 3rd-order dispersions are set to be $\pm$0.1, $\pm$0.2, $\pm$0.3, and $\pm$0.4 ps/nm^2.

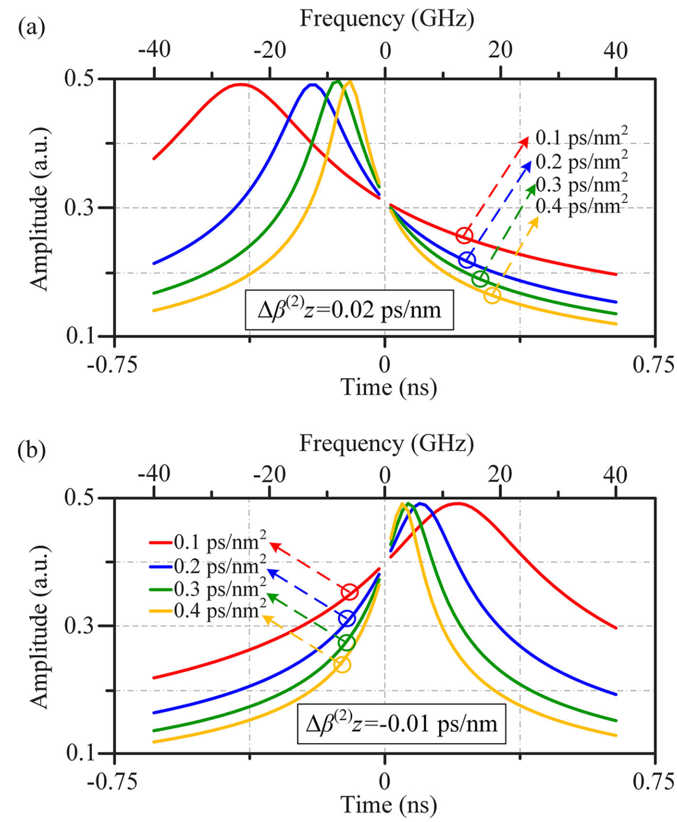

Fig. 9. The simulated envelopes of the RTFT results when the microwave signal frequency changes from 1 to 40 GHz under the condition that the values of the 3rd-order dispersions are set to be $\pm$0.1, $\pm$0.2, $\pm$0.3, and $\pm$0.4 ps/nm^2 with a residual 2nd-order dispersion of (a) 0.02 ps/nm and (b) -0.01 ps/nm.

that with the existence of the residual 2nd-order dispersion and the 3rd-order dispersion, the amplitude imbalance of the signal pulses located at the two sides of the reference pulse will be introduced, verifying the analyses provided in (9). At the same time, Fig. 9 also shows that the sign and values of *Disp*.3, *Disp.* 4 and *Disp.* 5 determine the position of the narrowest signal pulse, which has the largest amplitude and an optimal frequency resolution.

As shown in (9), the amplitude imbalance of the signal pulses located at the two sides of the reference pulse is caused by the different broadening of the signal pulses. The broadening of the signal pulses are determined by the spectrum bandwidth of the optical pulse [36] and the corresponding pulse broadening factors, which are $|\beta_0{}^{(3)}z(2\pi f)+\Delta\beta^{(2)}z|$ and $|\beta_0{}^{(3)}z(2\pi f)-\Delta\beta^{(2)}z|$, respectively. As a result, by reducing the spectrum bandwidth of the optical pulse, the amplitude imbalance of the signal pulses can be reduced. In the simulation, the spectrum bandwidth of the original pulse is changed from 40 nm to be 30, 20, 10, 5 nm, and the RTFT results of a single-frequency microwave signal with the frequency varying from 1 to 40 GHz are obtained. The corresponding envelopes are recorded, shown in Fig. 10. As can be seen, the amplitude imbalance of the signal pulses is eliminated with the decrease of the spectrum bandwidth of the optical pulse.

Based on the simulations, it can be seen that the frequency resolution of the RTFT system is degraded by the residual 2nd-order dispersion. A frequency-dependent power fading of the signal pulses is caused by the 3rd-order dispersion in the system. In addition, the joint effect of the residual 2nd-order dispersion and the 3rd-order dispersion causes the amplitude imbalance of the output signal pulses.

In order to solve these problems, an optical RTFT system based on a bidirectional CFBG and an optical filter is proposed with the schematic diagram shown in Fig. 11. An ultra-narrow optical pulse is filtered by an optical filter and injected into

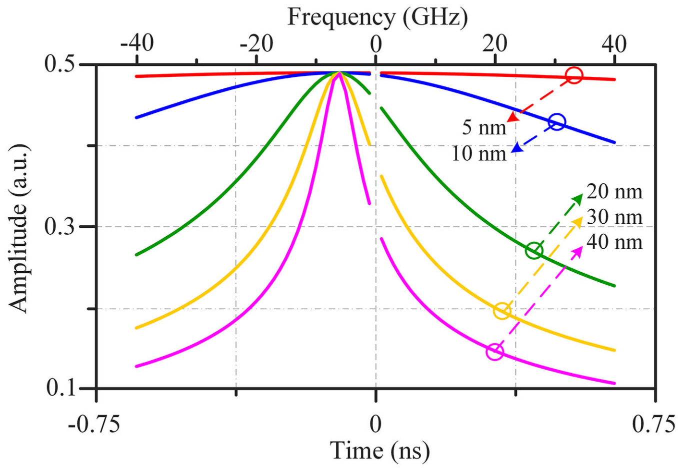

Fig. 10. The simulated envelopes of the RTFT results when the frequency of the modulated microwave signal changes from 1 to 40 GHz under the condition that the spectrum bandwidth of the optical pulse is set to be 5, 10, 20, 30, and 40 nm with a residual 2nd-order dispersion of 0.02 ps/nm and the 3rd-order dispersions of $\pm$0.4 ps/nm^2.

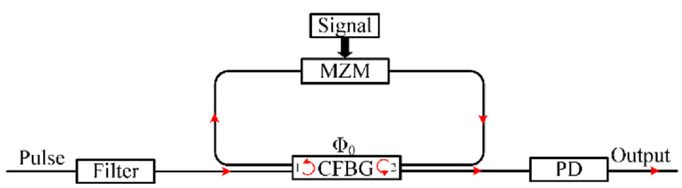

Fig. 11. Schematic diagram of the proposed RTFT system based on a bidirectional CFBG. CFBG: chirped Bragg fiber grating; MZM: Mach-Zehnder modulator; PD: photodetector.

port 1 of the bidirectional CFBG, reflected and output from the same port. The CFBG acts as a dispersion medium and the pulse is stretched in the time domain. Then the temporally stretched optical pulse is modulated by the electrical signal to be Fourier transformed via an MZM. The optical output of the MZM is injected to port 2 of the bidirectional CFBG, and reflected from the same port. After the optical-electrical conversion, the spectrum of the electrical signal is mapped into the time domain and the RTFT process is accomplished. Only one optical pulse source, a bidirectional CFBG, an MZM, and a PD are needed. The bidirectional CFBG offers complementary dispersions for the optical pulse propagating in the two opposite directions. Thus the effect of the residual 2nd-order dispersion with the frequency resolution of the system can be eliminated. Furthermore, by reducing the spectrum bandwidth of the optical pulse using an optical filter, amplitude imbalance of the signal pulses located at the two sides of the reference pulse can be reduced.

IV. Experimental Results

Based on the diagram, a proof-of-concept experiment is carried out. The experimental setup of the proposed system is illustrated in Fig. 12. An ultra-narrow optical pulse with a repetition of 10 MHz emitted from a mode-locked laser (Calmar) is filtered from 1528 nm to 1568 nm by a tunable optical filter

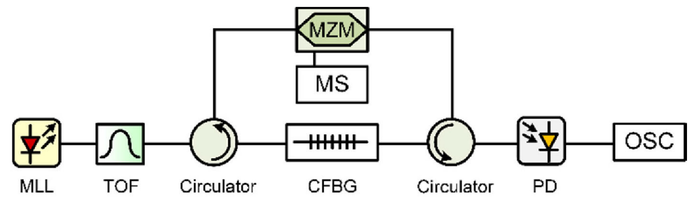

Fig. 12. Experimental setup. MLL: mode-locked laser; TOF: tunable optical filter; CFBG: chirped Bragg fiber grating; MZM: Mach-Zehnder modulator; MS: microwave source; PD: photodetector; OSC: oscilloscope.

(TOF, Finisar Waveshaper 4000S), satisfying the bandwidth of the bidirectional CFBG (Proximion AB Inc., wavelength range 1528–1568 nm). The dispersions of the bidirectional CFBG in the two opposite directions are 2000 and −2000 ps/nm, respectively, and the reflection losses in the two opposite directions are both 8 dB. After reflected and output from port 1 of the CFBG, the ultra-narrow optical pulse is temporally stretched. Then a microwave source (Agilent E8257D) is used to generate the electrical signal to be Fourier transformed, which is used to modulate the stretched optical signal via an MZM (Fujitsu, 40 GHz). The optical waveform output from the MZM is then injected into the port 2 of the bidirectional CFBG, reflected and then output from the same port. A sampling oscilloscope (Agilent Infiniium 86100C mainframe with 86116C module) is used to observe the temporal waveform of the optical signal. The working wavelength range is 1300-1620 nm, the bandwidth of the PD in 86116C module is 65 GHz, and the digitalization resolution is 14 bit. In the experiment, the optical spectra of the output signal are measured by an optical spectrum analyzer (Yokogawa AQ6370C) with a resolution of 0.02 nm. To compensate for the loss in the optical link, an erbium-doped fiber amplifier (EDFA) is inserted.

Before modulated by the signal to be measured, the filtered ultra-narrow pulse is firstly temporally stretched by the bidirectional CFBG. The optical spectrum and the temporal waveform of the stretched signal are shown in Fig. 13(a1) and Fig. 13(b1). As can be seen, the spectrum of the original optical pulse is mapped into the time domain. The time width of the stretched waveform is 80 ns, exactly the product of the spectrum width of the optical signal and the dispersion value of the CFBG, which are 40 nm and 2 ns/nm, respectively. The temporally stretched optical signal is modulated by an electrical signal with a frequency of 5 GHz and a power of 10 dBm. The optical spectrum and the temporal waveform of the output signal after the MZM are shown in Fig. 13(a2) and Fig. 13(b2), respectively. As can be seen, due to the frequency to time mapping, the spectrum of the optical signal is also temporally modulated by the 5-GHz electrical signal. As compared with Fig. 13(b2), the modulation detail in Fig. 13(a2) is not obvious, which is mainly due to the limited resolution of the used optical spectrum analyzer (0.02 nm in the experiment). Thus a zoom-in view is added to show the detail. By using an optical spectrum analyzer with a higher resolution, a finer optical spectrum with a visible modulation can be observed. By adjusting the MZM to work at the quadrature point and injecting the modulated stretched signal into port 2

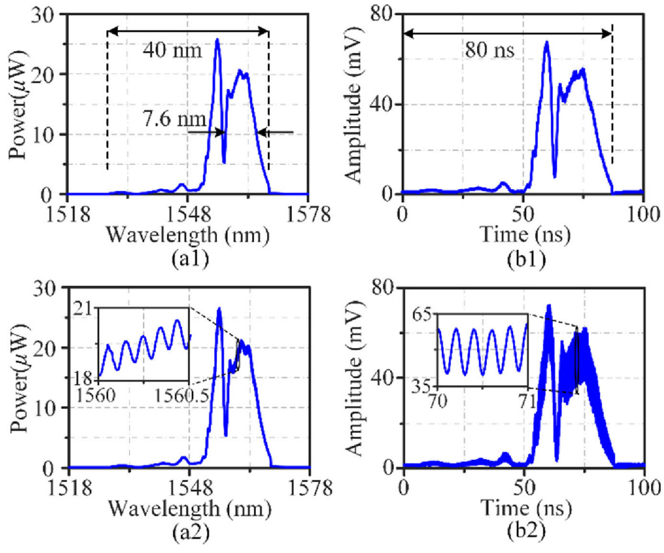

Fig. 13. (a) The optical spectrum and (b) the temporal waveform (1) before and (2) after the modulation by a 5-GHz electrical signal.

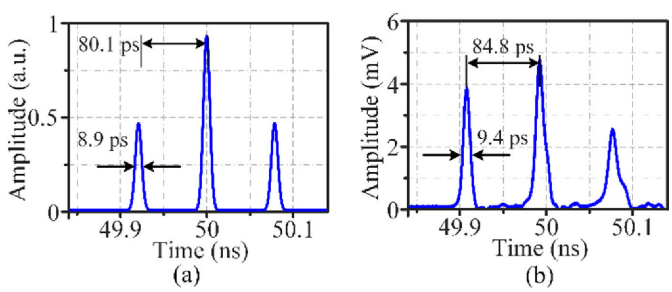

Fig. 14. (a) The simulated and (b) experimental RTFT result of a 5-GHz microwave signal.

of the CFBG, the spectrum of the electrical signal is mapped into the time domain. From Fig. 13(a1) we can see that the 3-dB spectrum bandwidth of the optical pulse in the experiment is only 7.6 nm, far from the operation bandwidth of the CFBG, which is 40 nm. The spectrum of the optical pulse is also not flat. In addition, due to the limited analog bandwidth and sampling rate, the minimum pulse width that can be distinguished by the OSC is only 8.9 ps. Considering these factors, a simulated RTFT result of the 5-GHz electrical signal is shown in Fig. 14(a). As a comparison, the experimental RTFT result is also shown in Fig. 14(b). From Fig. 14 we can see that two signal pulses appear at the two sides of the reference pulse. The time delay between the reference pulse and the signal pulses is about 80 ps, which is consistent with the product of the dispersion value and the frequency of the applied electrical signal. A good agreement between the simulation and the experiment is obtained.

In the photonics-based RTFT system, the spectrum of the electrical signal is linearly mapped into the time domain, thus a larger frequency corresponding to a larger time delay between the reference pulse and the signal pulse. To verify this, in the experiment, by changing the frequency of the electrical signal to

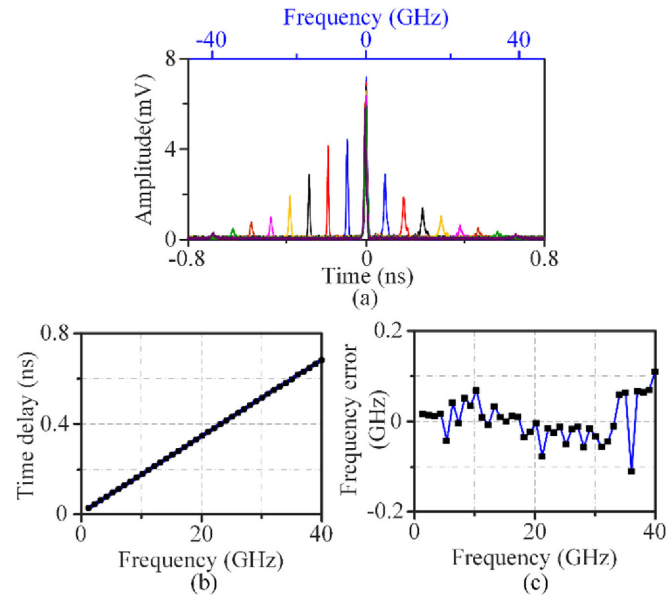

Fig. 15. (a) The experimental RTFT results of the single-frequency signal with the frequency varying from 5 to 40 GHz with a step of 5 GHz. (b) The experimental frequency to time mapping relationship and (c) the frequency error.

be Fourier transformed from 1 GHz to 40 GHz, the corresponding output waveforms are recorded. For a better illustration, Fig. 15(a) shows the RTFT results of the single-frequency signal when the frequency step is set to be 5 GHz, where different colors represent different frequencies. Time delays between the reference pulse and the signal pulses at different frequencies are measured and plotted in Fig. 15(b). By fitting the measured results, the frequency measurement error can be calculated, of which the result is shown in Fig. 15(c). It can be seen that the RTFT result has a linear mapping relationship from the frequency to the time domain, verifying the (4) and (5). The frequency measurement error in this experiment is shown to be ± 0.1 GHz. The sudden fall of the measurement error when the RF frequency is higher than 35 GHz is mainly due to the frequency response of the used MZM.

One key characteristic of the RTFT system is the frequency resolution, referring to the minimum frequency difference that can be distinguished, in other words, the minimum no-overlapping time interval when a two-tone signal is applied to the MZM. As shown in Fig. 14(b), when a 5-GHz electrical signal is applied to the system, the time width of the recompressed optical signal pulse is 9.4 ps. Considering the frequency-to-time mapping relationship, the frequency resolution will be 590 MHz, which is the ratio between the time width of the signal pulse and the dispersion value. By changing the frequency of the applied electrical signal and measuring the time width of the corresponding output recompressed signal pulse, the frequency resolution at different frequencies can also be obtained.

Experiments are also carried out to investigate the system performance of distinguishing two different frequencies. The results are shown in Fig. 16. When a two-tone microwave signal with frequencies of 10 and 11 GHz is applied to the MZM, the output RTFT result is shown in Fig. 16(a). As a comparison, the

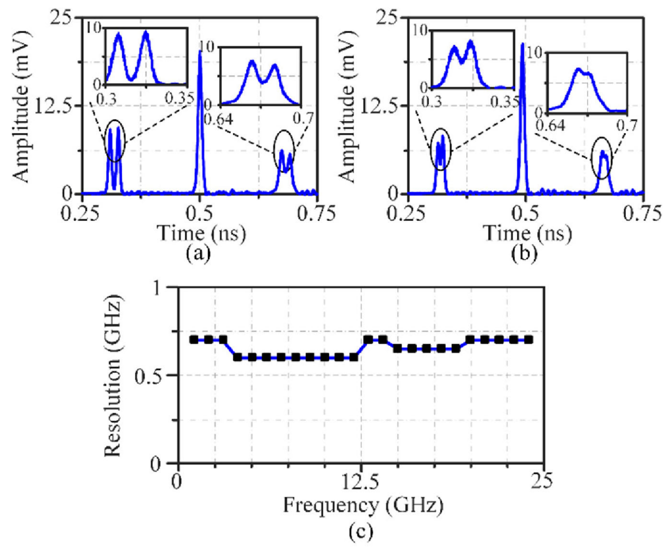

Fig. 16. Output waveforms of the RTFT results of a two-tone signal with the frequencies of (a) 10 GHz, 11 GHz and (b) 10 GHz, 10.6 GHz. (c) The frequency resolution at different frequencies.

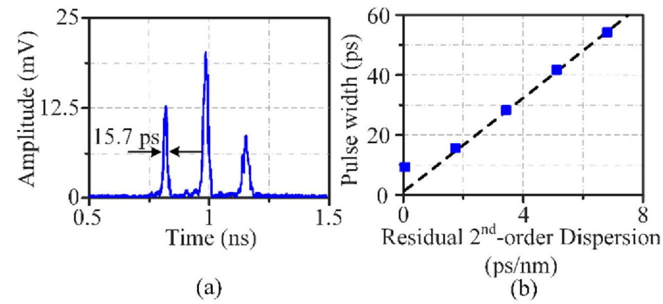

Fig. 17. (a) Output waveforms of the RTFT results of a 10-GHz microwave signal when adding single-mode fibers with a length of 100 m. (b) Relationship between the width of the recompressed pulse and the net dispersion in the system. Blue square dots: the experimental results, black dashed line: the simulated curve.

RTFT result of a two-tone microwave signal with frequencies of 10 and 10.6 GHz is also given in Fig. 16(b). As can be seen, when the frequency difference changes from 1 GHz to 0.6 GHz, the time interval of the generated two signal pulses is smaller. When the frequency difference decreases, the two signal pulses will overlap gradually, exceeding the resolution limit of the OSC. Thus the frequency resolution at 10 GHz is 0.6 GHz. The frequency resolutions at different frequencies are recorded and the results are plotted in Fig. 16(c). As can be seen, a frequency resolution of 700 MHz within the bandwidth of over 20 GHz is realized in this experiment.

A. Effect of the Residual 2nd-Order Dispersion

In the principle and simulation part, it has been analyzed that the time width of the recompressed pulse and the frequency resolution of the RTFT system are related to the match degree of the dispersion value before and after modulation. In order to verify the effect of the residual 2nd-order dispersion, an experiment is carried out. After the MZM, an extra SMF is inserted into the link to introduce the residual 2nd-order dispersions. When the frequency of the electrical signal is 10 GHz and the length of the SMF is 100 m, in other words, the extra dispersion is 1.7 ps/nm, corresponding RTFT result can be obtained, as shown in Fig. 17(a). By comparing Fig. 15(a) and Fig. 17(a), it can be seen that, due to the existence of the residual 2nd-order dispersion, the time width of the recompressed signal pulse is broadened from 9.1 ps to 15.7 ps. By changing the length of the SMF, the relationship between the width of the recompressed pulse and the net dispersion in the system can also be obtained, shown as the blue square dots in Fig. 17(b). As can be seen, when the value of the residual 2nd-order dispersion is larger, the time width of the recompressed pulse is also larger. Thus the frequency resolution will be degraded. By changing the value of the residual 2nd-order dispersion from 0 to 8 ps/nm, a simulation based on (7) is carried out, with the result shown as the black dashed line in Fig. 17(b). A good agreement between the simulation and the experimental results has been achieved. When the residual 2nd-order dispersion is close to 0, the error becomes large, due to the limited analog bandwidth and sampling rate of the OSC.

B. Amplitude Imbalance of the Sideband Pulses

A non-ignorable phenomenon in the RTFT results shown in Fig. 15 is that when a single-frequency electrical signal is applied, the amplitudes of the recompressed two signal pulses are different, as shown in the figures before. Principle and simulations have shown that the amplitude imbalance of sideband pulses comes from the joint effect of the residual 2nd-order dispersion and the 3rd-order dispersion. Here we explain the time width difference and the amplitude difference of the recompressed signals as follows. Due to the modulation process, for example, a 5-GHz microwave signal is modulated to the stretched optical pulse, the frequency shifts of ±5 GHz are introduced to the spectrum of the optical signal, which leads to the generation of the two recompressed pulses. Because of the residual 2nd-order dispersion and the 3rd-order dispersion of the CFBG, the ±5 GHz frequency-shifted spectra will undergo different net dispersions. Thus the generated two signal pulses have different pulse widths and different pulse amplitudes.

Theoretically, the amplitude difference and the time width difference of the generated two signal pulses are related to the dispersion difference that the ±5 GHz frequency-shifted sidebands undergo and the spectrum bandwidth of the optical pulse signal. Thus using the method in [37], the group delay of the CFBG is firstly measured and the 2nd-order dispersion values of the two directions of the CFBG are calculated. Corresponding results are shown in Fig. 18(a). As can be seen, the 2nd-order dispersion values of the two directions of the CFBG are opposite. Meanwhile, the 3rd-order dispersion also exists. Utilizing the measurement data, the 3rd-order dispersions are also calculated. The residual 2nd-order dispersion value is measured to be -0.8 ps/nm, which is much smaller than the 2nd-order dispersion values of the CFBG (±2000 ps/nm), with the relative residual ratio only to be 0.4‰. The 3rd-order dispersion values of the

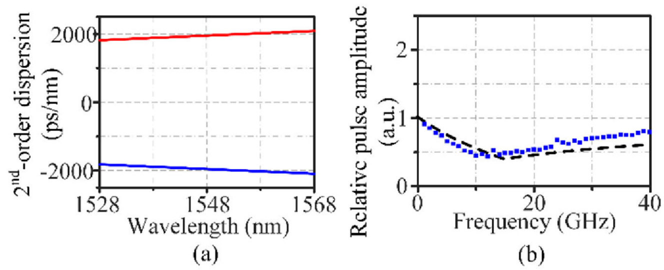

Fig. 18. (a) Measurement results of the 2nd-order dispersion of the two directions in the CFBG, red line: positive dispersion, blue line: negative dispersion. (b) The theoretical simulated curve (black dashed line) and the experimental results (blue square dots) of the relative pulse amplitude versus the microwave signal frequency.

CFBG are measured to be ± 6.8 ps/nm^2. To evaluate the amplitude imbalance of sideband pulses, relative pulse amplitude is introduced, which refers to the ratio of the signal pulse amplitudes at the two sides of the reference pulse. Thus the amplitudes of the signal pulses in Fig. 15(a) are measured, and the experimental results of the relative pulse amplitude of the two signal pulses versus microwave signal frequency can be calculated, which is plotted as the blue square dots in Fig. 18(b). For a comparison, using the obtained dispersion values in Fig. 18(a), the relationship between the theoretical relative pulse amplitude of the two signal pulses and the microwave signal frequency can be calculated, of which the result is shown as the black dashed line in Fig. 18(b). A good agreement between the simulation results and the experimental results has been realized.

Simulations have shown that a smaller spectrum bandwidth of the optical pulse will reduce the amplitude imbalance of the sideband pulses appearing at the two sides of the reference pulse. In order to verify this, in the experiment, we adjust the bandwidth of the optical filter after the MLL to be 40 nm and 2 nm, the corresponding RTFT results of a microwave signal with a frequency of 20 GHz are shown in Fig. 19(a) and Fig. 19(b). Diagram of the relationship between the relative pulse amplitude of the two signal pulses and the spectrum bandwidth of the optical pulse is plotted as the blue square dots in Fig. 19(c). As a comparison, the simulated result based on (9) is also given as the black dashed line in Fig. 19(c). A good agreement between the simulation and the experimental results has been shown. It can be seen from Fig. 19 that as the bandwidth of the optical signal decreases, the amplitude imbalance of the two signal pulses can be eliminated.

C. Dynamic Range

Finally, the dynamic range of the system is also investigated by changing the power of the input RF signal and measuring the amplitude of the output pulses. The corresponding result is depicted as the blue square dots in Fig. 20. A linear fitting method is used and the fitting result is plotted as the black dashed line in Fig. 20. The frequency of the electrical signal applied to the MZM is 5 GHz. It can be seen that when the input power increases from 9 to 17 dBm with a step of 1 dBm, the output power is approximately linearly increased. When the power of

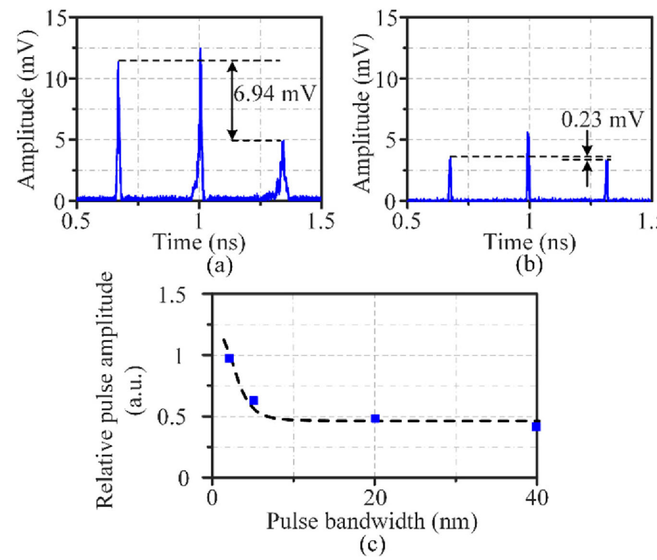

Fig. 19. RTFT results of a 20-GHz microwave signal when the spectrum bandwidth of the optical signal is (a) 40 nm, (b) 2 nm. (c) Relationship between relative pulse amplitude and spectrum bandwidth of the optical pulse. Blue square dots: the experimental results. Black dashed line: the simulated curve.

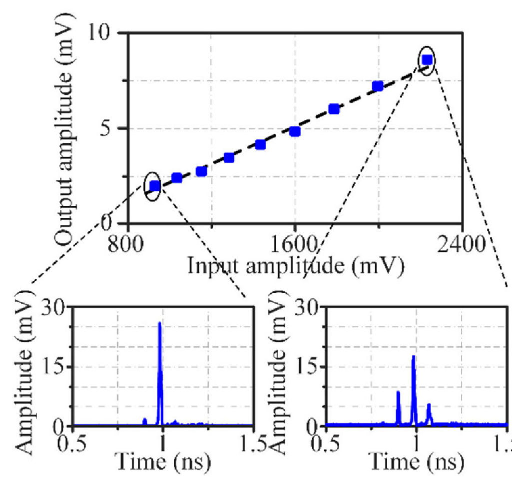

Fig. 20. (a) The relationship between the amplitude of the RF signal and the amplitude of the output signal pulse. Blue square dots: experimental results. Black dashed line: fitting result.

the input signal is much higher, the condition of small-signal approximation is not applicable and the harmonic will appear. When the power of the input signal is below 9 dBm, the output signal pulses will be submerged by the noise of the system. Thus a dynamic range of 12-dB is achieved.

V. Discussions

In the parts of principle and experimental results, we have demonstrated that the existence of the 3rd-order dispersion will cause the amplitude fading of the output pulses versus the frequency of the microwave signal, theoretically shown in (8) and (9). In fact, considering the frequency-dependent response of the modulator, the same power of the microwave signal will introduce different modulation depths. Thus β_m in the above equations is also a frequency-dependent parameter, which will also affect the amplitude fading of the output signal pulses. To eliminate the amplitude fading effect introduced by the frequency-dependent modulation depth, the response of the modulator can be measured in advance and a post-processing method to compensate the fading can be applied. To further solve the amplitude fading effect, precise dispersion management to eliminate the 3rd-order dispersion in the system can be considered. On the other hand, as shown in Fig. 6(c), the ideal frequency resolution of the proposed RTFT system is 11.25 MHz, which is the ratio between the time width of the original optical pulse and the 2nd-order dispersion value of the CFBG. However, because of the limited analog bandwidth of the ADC in the OSC, the time resolution, which is mapped from the frequency resolution, is not able to be distinguished. Another important characteristic of the system is the bandwidth. Theoretically, the bandwidth of the RTFT system is the ratio of the non-overlapping temporal interval of the signal pulses and the frequency-to-time mapping factor. In this experiment, considering the double-sideband modulation, the non-overlapping temporal interval is half of the MLL's repetition period, which is 50 ns in the experiments. Thus the ideal bandwidth of the proposed RTFT system is 3125 GHz. However, the practical bandwidth is limited by the bandwidth of the MZM, which is 40 GHz in this experiment, shown in Fig. 15. By using modulators with larger bandwidths, the bandwidth of the system can be further extended. In addition, the total power loss introduced by the CFBG and the MZM is about 25 dB. Thus the system efficiency can be improved by introducing an MZM and a CFBG with low insertion loss. For the dynamic range performance of the system, the minimum microwave signal that can be observed by the system is determined by the loss of the link, the dark current in the PD and the digitalization resolution of the oscilloscope. The maximal microwave signal that can be measured is determined by the half-wave voltage of the MZM and the saturated optical power of the PD. These parameters will influence the dynamic range of the system, which can be improved by using a CFBG with a higher reflectivity [38], and implementing the optical power control of the system. Furthermore, the system can be made to be more compact with the development of the integrated microwave photonics [39].

VI. Conclusion

In conclusion, we have theoretically analyzed the impact of dispersion effects on the photonics-based RTFT system. The existence of the residual 2nd-order dispersion causes the broadening of the output signal pulses and the frequency resolution degradation of the system; the 3rd-order dispersion and the frequency-dependent response of the MZM cause the amplitude fading of the signal pulses with the frequency of the modulated microwave signal; the joint effect of the residual 2nd-order dispersion and the 3rd-order dispersion causes the amplitude imbalance of the output signal pulses. In order to solve these problems, a CFBG with complementary dispersions for temporal stretching and compression, precise dispersion management together with a post-processing algorithm utilizing the frequency response of the modulator, and the decrease of the spectrum bandwidth of the optical pulse, can be applied, respectively. Mathematical simulations and proof-of-concept experiments are carried out. In the experiment, a frequency resolution of 0.7 GHz and a bandwidth of 40 GHz have been experimentally verified. With the help of a high-speed oscilloscope and a modulator with larger bandwidth, a frequency resolution of 11.25 MHz and a bandwidth of larger than 3 THz are theoretically achievable. These analyses and the proposed photonics-based RTFT system based on the bidirectional CFBG can find applications in the areas of spectrum measurement systems and electrical warfare and so on.

References

[1] A. E. Spezio, "Electronic warfare systems," *IEEE Trans. Microw. Theory Techn.*, vol. 50, no. 3, pp. 633–644, Mar. 2002.

[2] F. Z. Zhang, Q. S. Guo, and S. L. Pan, "Photonics-based real-time ultra-high-range-resolution radar with broadband signal generation and processing," *Sci. Rep.*, vol. 7, Oct. 2017, Art. no. 13848.

[3] G. G. Raleigh and J. M. Cioffi, "Spatio-temporal coding for wireless communication," *IEEE Trans. Commun.*, vol. 46, no. 3, pp. 357–366, Mar. 1998.

[4] T. Jannson, "Real-time Fourier transformation in dispersive optical fibers," *Opt. Lett.*, vol. 8, no. 4, pp. 232–234, Apr. 1983.

[5] K. Goda and B. Jalali, "Dispersive Fourier transformation for fast continuous single-shot measurements," *Nat. Photon.*, vol. 7, no. 2, pp. 102–112, Jan. 2013.

[6] K. Goda, D. R. Solli, K. K. Tsia, and B. Jalali, "Theory of amplified dispersive Fourier transformation," *Phys. Rev. A*, vol. 80, no. 4, pp. 82–82, Oct. 2009.

[7] J. Azana, L. R. Chen, M. A. Muriel, and P. W. E. Smith, "Experimental demonstration of real-time Fourier transformation using linearly chirped fibre Bragg gratings," *Electron. Lett.*, vol. 35, no. 25, pp. 2223–2224, Dec. 1999.

[8] J. Azana and M. A. Muriel, "Dual-channel real-time Fourier transformer based on chirped Moiré fiber grating," in *Proc. Bragg Gratings, Photosensitivity, Poling Glass Waveguides*, 1999, Paper AD3.

[9] M. A. Muriel, J. Azana, and A. Carballar, "Real-time Fourier transformer based on fiber gratings," *Opt. Lett.*, vol. 24, no. 1, pp. 1–3, Jan. 1999.

[10] J. Azana, M. A. Muriel, and A. Carballar, "Real-time fourier transformer system using transmissive fiber gratings," *Fiber Integr. Opt.*, vol. 19, no. 4, pp. 439–453, Oct. 2000.

[11] J. Azana and M. A. Muriel, "Real-time optical spectrum analysis based on the time-space duality in chirped fiber gratings," *IEEE J. Quantum Electron.*, vol. 36, no. 5, pp. 517–526, May 2002.

[12] B. Kolner, "Space-time duality and the theory of temporal imaging," *IEEE J. Quantum Electron.*, vol. 30, no. 8, pp. 1951–1963, Aug. 1994.

[13] J. Azana, N. K. Berger, B. Levit, and B. Fischer, "Spectro-temporal imaging of optical pulses with a single time lens," *IEEE Photon. Technol. Lett.*, vol. 16, no. 3, pp. 882–884, Mar. 2004.

[14] C. Xu and J. V. Howe, "Ultrafast optical signal processing based upon space-time dualities," *J. Lightw. Technol.*, vol. 24, no. 7, pp. 2649–2662, Jul. 2006.

[15] F. Yin, J. Li, K. Xu, Y. Zheng, and Y. Dai, "Real-time Fourier transformation based on the bandwidth magnification of RF signals," *Opt. Lett.*, vol. 43, no. 2, pp. 194–197, Jan. 2018.

[16] C. Zhang, X. Wei, M. E. Marhic, and K. K. Y. Wong, "Ultrafast and versatile spectroscopy by temporal Fourier transform," *Sci. Rep.*, vol. 4, Jun. 2014, Art. no. 5351.

[17] R. Salem, M. A. Foster, and A. L. Gaeta, "Application of space–time duality to ultrahigh-speed optical signal processing," *Adv. Opt. Photon.*, vol. 5, pp. 274–317, Aug. 2013.

[18] H. G. D. Chatellus, L. R. Cortés, and J. Azaña, "Optical real-time Fourier transformation with kilohertz resolutions," *Optica*, vol. 3, no. 1, pp. 1–8, Jan. 2016.

[19] C. Schnébelin and H. G. D. Chatellus, "Agile photonic fractional Fourier transformation of optical and RF signals," *Optica*, vol. 4, no. 8, pp. 907–910, Aug. 2017.

[20] H. G. de Chatellus, L. R. Cortés, C. Schnébelin, M. Burla, and J. Azaña, "Reconfigurable photonic generation of broadband chirped waveforms using a single CW laser and low-frequency electronics," *Nat. Commun.*, vol. 9, no. 1, Jun. 2018, Art. no. 2438.

[21] V. Durán, C. Schnébelin, and H. G. de Chatellus, "Coherent multi-heterodyne spectroscopy using acousto-optic frequency combs," *Opt. Express*, vol. 26, no. 11, pp. 13800–13809, May 2018.

[22] V. Durán *et al.*, "Optical frequency combs generated by acousto-optic frequency-shifting loops," *IEEE Photon. Technol. Lett.*, vol. 31, no. 23, pp. 1878–1881, Oct. 2019.

[23] C. Schnébelin, J. Azaña, and H. G. de Chatellus, "Programmable broad-band optical field spectral shaping with megahertz resolution using a simple frequency shifting loop," *Nat. Commun.*, vol. 10, no. 1, pp. 1–11, Oct. 2019.

[24] R. E. Saperstein, D. Panasenko, and Y. Fainman, "Demonstration of a microwave spectrum analyzer based on time-domain optical processing in fiber," *Opt. Lett.*, vol. 29, no. 5, pp. 501–503, Mar. 2004.

[25] H. Chi and J. Yao, "Waveform distortions due to second-order dispersion and dispersion mismatches in a temporal pulse-shaping system," *J. Lightw. Technol.*, vol. 25, no. 11, pp. 3528–3535, Nov. 2007.

[26] H. Sun, X. Zhu, W. Li, N. Zhu, and M. Li, "Real-time optical spectrum Fourier transform with time–bandwidth product compression," *IEEE Photon. J.*, vol. 10, no. 1, pp. 1–14, Feb. 2018.

[27] M. Li, C. Wang, W. Li, and J. Yao, "An imbalanced temporal pulse-shaping system for chirped microwave waveform generation," *IEEE Trans. Microw. Theory Techn.*, vol. 58, no. 11, pp. 2968–2975, Nov. 2010.

[28] M. Li, Y. Han, S. Pan, and J. Yao, "Experimental demonstration of symmetrical waveform generation based on amplitude-only modulation in a fiber-based temporal pulse shaping system," *IEEE Photon. Technol. Lett.*, vol. 23, no. 11, pp. 715–717, Jun. 2011.

[29] C. Wang, "Dispersive fourier transformation for versatile microwave photonics applications," *Photonics*, vol. 1, no. 4, pp. 586–612, Dec. 2014.

[30] W. T. Wang, M. Li, S. Q. Sun, C. Wang, Y. Deng, and N. H. Zhu, "Background-free microwave signal generation based on imbalanced temporal pulse shaping," *IEEE Photon. Technol. Lett.*, vol. 28, no. 8, pp. 903–906, Apr. 2016.

[31] L. Chen, Y. Duan, C. Zhang, and X. Zhang, "Frequency-domain light intensity spectrum analyzer based on temporal convolution," *Opt. Lett.* vol. 42, no. 14, pp. 2726–2729, Jul. 2017.

[32] S. Wang *et al.*, "Photonic compressive receiver for multiple microwave frequency measurement." *Opt. Express*, vol. 27, no. 18, pp. 25364–25374, Sep. 2019.

[33] Y. H. Duan, L. Chen, H. D. Zhou, X. Zhou, C. Zhang, and X. L. Zhang, "Ultrafast electrical spectrum analyzer based on all-optical Fourier transform and temporal magnification," *Opt. Express*, vol. 25, no. 7, pp. 7520–7529, Apr. 2017.

[34] Y. H. Duan, L. Chen, L. Zhang, X. Zhou, C. Zhang, and X. L. Zhang, "Temporal radio-frequency spectrum analyzer, based on asynchronous optical sampling assisted temporal convolution," *Opt. Express*, vol. 26, no. 16, pp. 20735–20743, Aug. 2018.

[35] M. Miyagi and S. Nishida, "Pulse spreading in a single-mode fiber due to third-order dispersion," *Appl. Opt.*, vol. 18, no. 5, pp. 678–682, Mar. 1979.

[36] G. P. Agrawal, *Application of Nonlinear Fiber Optics*, San Diego, CA: Academic Press, 2001.

[37] R. Fortenberry, W. V. Sorin, and P. Hernday, "Improvement of group delay measurement accuracy using a two-frequency modulation phase-shift method," *IEEE Photon. Technol. Lett.*, vol. 15, no. 5, pp. 736–738, Jun. 2003.

[38] L. Wang *et al.*, "Wavelength-swept fiber laser based on bidirectional used linear chirped fiber Bragg grating," *Photon. Res.*, vol. 5, no. 3, pp. 219–223, Jun. 2017.

[39] D. Marpaung, C. Roeloffzen, R. Heideman, A. Leinse, S. Sales, and J. Capmany, "Integrated microwave photonics," *Laser Photon. Rev.*, vol. 7, no. 4, pp. 506–538, Jul. 2013.

Bowen Zhang received the B.S. degree in electronics engineering from Tsinghua University, Beijing, China, in 2016. He is currently working toward the Ph.D. degree with the Key Laboratory of Radar Imaging and Microwave Photonics, the Ministry of Education, Nanjing University of Aeronautics and Astronautics, Nanjing, China. His research interests include photonic microwave measurement and photonic technologies for microwave signal processing.

Dan Zhu (Member, IEEE) received the B.S. and Ph.D. degrees in electronics engineering from Tsinghua University, Beijing, China, in 2004 and 2009, respectively. In July 2009, she joined the Research Department of Radar Signal Processing, No. 14 Research Institute, China Electronics Technology Group Corporation, as a Researcher. In May 2011, she joined the Key Laboratory of Radar Imaging and Microwave Photonics, Ministry of Education, Nanjing University of Aeronautics and Astronautics, Nanjing, China, where she is now an Associate Professor. Her current research interests include microwave photonic signal processing and the system applications. Dr. Zhu is a member of the IEEE Microwave Theory and Techniques Society, the IEEE Photonics Society, and a member of the Optical Society of America.

Zhen Lei, biography not available at the time of publication.

Zhongyang Xu received the B.S. degree in physics from Sun Yat-sen University, Guangzhou, China, in 2010 and the Ph.D. degree in physics from Tsinghua University, Beijing, China, in 2015. He is currently a Lecturer with the Key Laboratory of Radar Imaging and Microwave Photonics, Ministry of Education, Nanjing University of Aeronautics and Astronautics, Nanjing, China. His current research interests are in frequency-modulated continuous-wave detection and radio over free-space optics.

Tao Zhou, biography not available at the time of publication.

Xin Zhong, biography not available at the time of publication.

Zhiyu Chen, biography not available at the time of publication.

Shilong Pan (Senior Member, IEEE) received the B.S. and Ph.D. degrees in electronic engineering from Tsinghua University, Beijing, China, in 2004 and 2008, respectively. From 2008 to 2010, he was a "Vision 2010" Postdoctoral Research Fellow with the Microwave Photonics Research Laboratory, University of Ottawa, Canada. He joined the College of Electronic and Information Engineering, Nanjing University of Aeronautics and Astronautics, China, in 2010, where he is currently a Full Professor and an Executive Director of the Key Laboratory of Radar Imaging and Microwave Photonics, the Ministry of Education. His research has focused on microwave photonics, which includes optical generation and processing of microwave signals, analog photonic links, photonic microwave measurement, and integrated microwave photonics. Prof. Pan has authored or co-authored over 420 research papers, including more than 240 papers in peer-reviewed journals and 190 papers in conference proceedings. Prof. Pan is currently an Associate Editor of *Electronics Letters*, a Topical Editor of *Chinese Optics Letters*, and is a Technical Committee member of *IEEE MTT-3 Microwave Photonics*. He has also served as a Chair of a number of international conferences, symposia, and workshops, including the TPC Chair of the International Conference on Optical Communications and Networks in 2015, and TPC Co-chair of IEEE International Topical Meeting on Microwave Photonics in 2017. Prof. Pan is a Fellow of OSA, SPIE and IET, and a Senior Member of IEEE. He was selected as an IEEE Photonics Society Distinguished Lecturer in 2019.